



Published in final edited form as:

Chem. 2016 September 8; 1(3): 456–472. doi:10.1016/j.chempr.2016.08.002.

## Photochemical Perfluoroalkylation with Pyridine *N*-Oxides: Mechanistic Insights and Performance on a Kilogram Scale

Joel W. Beatty<sup>1</sup>, James J. Douglas<sup>2</sup>, Richard Miller<sup>2</sup>, Rory C. McAtee<sup>1</sup>, Kevin P. Cole<sup>2</sup>, and Corey R.J. Stephenson<sup>1,\*</sup>,<sup>3</sup>

<sup>1</sup>Department of Chemistry, University of Michigan, Ann Arbor, MI 48109, USA

<sup>2</sup>Small Molecule Design and Development, Lilly Research Laboratories, Eli Lilly and Company, Indianapolis, IN 46285, USA

### SUMMARY

The direct trifluoromethylation of (hetero)arenes is a process of high importance to the pharmaceutical industry. Many reagents exist for this purpose and have found widespread use in discovery efforts; however, the step-intensive preparation of these reagents and their corresponding cost have resulted in minimal use of these methods in large-scale applications. For the ready transition of direct trifluoromethylation methodologies to large-scale application, the further development of processes utilizing inexpensive CF<sub>3</sub> sources available on a metric ton scale is highly desirable. We report the use of pyridine *N*-oxide derivatives in concert with trifluoroacetic anhydride to promote a high-yielding and scalable trifluoromethylation reaction. Key mechanistic insights include the observation of electron donor-acceptor complexes in solution as well as a high dependence on photon flux. These observations have culminated in the application of this chemistry on a kilogram scale, demonstrating the utility of this reagent combination for preparative applications.

### Graphical abstract

\*Correspondence: crjsteph@umich.edu.

<sup>3</sup>Lead Contact

#### ACCESSION NUMBERS

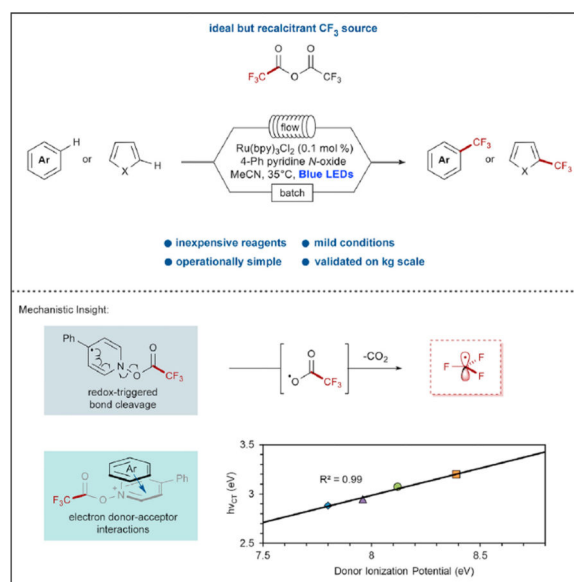
The structure of pyrrolidine **17** in this article has been deposited in the Cambridge Crystallographic Data Center under accession number CCDC: 1485256.

#### SUPPLEMENTAL INFORMATION

Supplemental Information includes Supplemental Experimental Procedures, 41 figures, and 1 data file and can be found with this article online at <http://dx.doi.org/10.1016/j.chempr.2016.08.002>.

#### AUTHOR CONTRIBUTIONS

J.W.B., J.J.D., R.M., and R.C.M. performed the experiments; J.W.B., J.J.D., K.P.C., and C.R.J.S. designed the experiments and analyzed the data. J.W.B., J.J.D., K.P.C., and C.R.J.S. wrote the manuscript.



Fluorine incorporation has become a highly important feature of drug-synthesis technology in recent decades. Although a multitude of methods have been developed for small-scale discovery efforts, direct, truly scalable perfluoroalkylation has been generally limited to reactions involving superstoichiometric amounts of copper. In an effort to minimize the associated environmental cost of these processes, Stephenson and colleagues demonstrate an improved perfluoroalkylation method requiring minimal catalyst loadings and utilizing visible light on a kilogram scale.

## INTRODUCTION

The unique influence of fluorine incorporation on metabolic stability, lipophilicity, and pharmacokinetics has elevated organofluorine chemistry to a central role in the design of pharmaceuticals<sup>1</sup> and agrochemicals.<sup>2</sup> Since the late 1950s, fluorinated drugs have consisted of roughly 5%–15% of newly launched pharmaceuticals on a yearly basis,<sup>3</sup> and about 200 fluorine-containing drugs have been approved to date.<sup>4</sup> Commodity trifluoromethylated arenes are produced industrially through direct halogen-fluoride exchange of benzotrifluorides; however, this process is limited to methylated arenes of significant oxidative and thermal stability, which are chlorinated before being subjected to anhydrous hydrogen fluoride at elevated temperatures.<sup>5</sup> Alternative strategies are required to produce electron-rich and acid-sensitive benzotrifluorides, and halogen-fluoride exchange is not effective for higher-order perfluoroalkyl groups such as C<sub>2</sub>F<sub>5</sub>. Because of the challenges and limited substrate scope associated with direct C–F bond formation, many reagents for the direct incorporation of fluorinated groups have found widespread synthetic utility and strategic relevance.<sup>6</sup> This is particularly true for trifluoromethylation reagents,<sup>7</sup> which can be used to accomplish fluoroalkylations through nucleophilic,<sup>8–15</sup> electrophilic,<sup>16–20</sup> or radical<sup>21–36</sup> additions of CF<sub>3</sub> and are likewise used broadly in cross-coupling applications.<sup>37–43</sup>

Despite the undeniable value and utility of these compounds for discovery research, the use of many of these reagents in large-scale applications becomes less appealing when issues of

reagent cost, environmental impact, and material sourcing are considered. Trifluoroacetic acid (TFA) and fluoroform ( $\text{HCF}_3$ ) are the most attractive  $\text{CF}_3$  source materials in these respects because they are inexpensive and available in large quantities; furthermore, the majority of reagents for trifluoromethylation are prepared from these materials, and the environmental impact of the direct use of TFA or  $\text{HCF}_3$  is consequently minimal in comparison. The use of  $\text{HCF}_3$  has been pioneered by Grushin for the preparation of  $\text{CuCF}_3$  in high yields; it can be used in a mild, room-temperature trifluoromethylation of both halides and boronic acids.<sup>39,44,45</sup> Conversely, a broadly applicable and mild utilization of TFA as a  $\text{CF}_3$  source has been slower to develop, given that forcing conditions have traditionally been required to promote this reactivity.

The ability to directly oxidize trifluoroacetate has yet to be accomplished by redox-based photocatalysis; this is a result of the high oxidation potential of trifluoroacetate, which is observed for the sodium salt at potentials greater than +2.4 V versus saturated calomel electrode (SCE) in MeCN.<sup>46</sup> These electrochemical potentials limit the compatibility of direct TFA oxidation with many substrates and solvents, and an alternative strategy is required for true synthetic utility. Matsui was the first to report the trifluoromethylation of aryl halides using sodium trifluoroacetate and superstoichiometric copper and noted that the polar decarboxylation of this salt was observed at temperatures above 140°C in the presence of CuI (Scheme 1).<sup>47</sup> Subsequent work by Buchwald has demonstrated that this reactivity can be accelerated significantly at increased temperatures.<sup>48</sup> Open-shell pathways for decarboxylation through oxidation to the corresponding carboxyl radical have been accomplished with relatively few reagents, including  $\text{XeF}_2$ ,<sup>49</sup> mixtures of silver salts and persulfate,<sup>50</sup> and the UV-promoted decarboxylation of silver trifluoroacetate.<sup>51</sup> The requisite strength of these oxidants has limited the substrate scope of such transformations to electron-poor compounds to minimize their background degradation. A sole and notable exception to this theme is Sawada's use of bis(trifluoroacetyl) peroxide (Scheme 1), which, despite the use of Freon 113 (1,1,2-trichloro-1,2,2-trifluoroethane) as a solvent, has been shown to be the only TFA derivative capable of trifluoromethylating electron-rich heterocycles such as furans and thiophenes.<sup>52,53</sup>

Visible-light photoredox catalysis has shown remarkable utility for decarboxylative chemistry, with a number of leading examples from MacMillan,<sup>54–60</sup> Wallentin,<sup>61</sup> and Nicewicz<sup>62</sup> demonstrating the feasibility and compatibility of this approach. As a general principle, these methods involve the direct oxidation of a carboxylate by a redox-active photocatalyst and are limited to electron-rich aliphatic carboxylates with minimal exception.<sup>63</sup> Our interest in visible-light-mediated processes led us to pursue a photochemical means for the radical decarboxylation of trifluoroacetate derivatives, which optimally would be safely scalable, promoted within a readily accessible redox window, and occur at ambient temperature. We recently reported such a method through the use of pyridine *N*-oxide as a stoichiometric redox trigger to facilitate the photochemical decarboxylation of trifluoroacetic anhydride (TFAA).<sup>64</sup> As a conceptual alternative to direct carboxylate oxidation, the acylation of a pyridine *N*-oxide derivative allows the reaction manifold to be accessed through a reductive pathway. This design expands the scope of photoredox-mediated decarboxylation to electron-poor carboxylates, and through this method, a number of electron-rich and redox-sensitive substrates have been

trifluoromethylated using TFAA. At the outset of this work, the use of pyridine *N*-oxide remained untested for scale-up applications beyond 20 g, and the yields of this process were not competitive with those of popular and established trifluoromethylation methods such as MacMillan's use of trifluoromethanesulfonyl chloride with photoredox catalysis<sup>26</sup> or Baran's Zn(O<sub>2</sub>SCF<sub>3</sub>)<sub>2</sub>/tBuOOH system.<sup>29,30</sup> Driven by an improved mechanistic understanding of this process, we have identified 4-phenylpyridine *N*-oxide as an efficient redox trigger with correspondingly improved reaction yields and detail the application of this methodology on a 1.2 kg scale in a photochemical flow reactor.

## RESULTS AND DISCUSSION

### Optimization of *N*-Oxide Electronics

Although pyridine *N*-oxide is readily available and presents minimal cost when implemented on scale, we recognized that the electronics of the *N*-oxide are influential in determining reactivity. Both the redox potential of the *N*-oxide/TFAA adduct and the affinity of the CF<sub>3</sub> radical for the pyridine byproducts could be tuned through pyridine functionalization, and other mechanistic factors including reaction quantum yield and fluorescence quenching rates are expected to be influenced by these changes. Electron-poor and highly conjugated *N*-oxides are expected to be more readily reduced, and so using mesitylene (**2**) as the model substrate, we began by investigating a number of electronically tuned pyridine *N*-oxides. This process initially yielded mixed results, such that a large number of pyridine derivatives proved less efficient than pyridine *N*-oxide itself (Table 1, entries 1–12). Inclusion of electron-withdrawing substituents did not improve reaction efficiency (entries 2–4), and electron-donating substituents were equally ineffective (entries 5–7). Alkyl pyridines with substituents in the 2 and 4 positions are well-known substrates of the Boekelheide reaction, and as such were excluded from our investigation.<sup>65</sup> Improved results were obtained when 4-phenylpyridine *N*-oxide (**1**) was used, providing 10% more mono-functionalized mesitylene (entry 9). Alternative biaryl *N*-oxides did not perform as efficiently (entries 10–12).

Exclusion of the catalyst from these reaction conditions was found to provide only trace amounts of **2** when 4-phenylpyridine *N*-oxide was used (entries 13 and 14), and increased equivalents of *N*-oxide and TFAA in the presence of catalyst resulted in improvements to the overall yield, with concomitant increases in the amount of **2b** formed (entries 15 and 16). The formation of **2b** resulted from further functionalization of **2** and as such was not considered a drawback at this point of reaction development. Degassing of the reaction solution was found to improve the yield of functionalized mesitylene (entries 17–18); the magnitude of improvement resulting from the exclusion of oxygen has been found to be both *N*-oxide and substrate dependent. Lowering the catalyst loading to 0.1 mol % resulted in comparable yields (entries 19 and 20). Control experiments demonstrated that visible-light irradiation in the absence of oxygen and catalyst promoted an appreciable background reaction with **1** (entries 21 and 22), whereas complete exclusion of light provided no reactivity (entry 23). It should be noted that this background reactivity is predicated on the degassing of the solution (entry 14 versus 21), and background trifluoromethylation is only at trace levels with unfunctionalized pyridine *N*-oxide. It is also clear that the formation of **2b** is an artifact of substrate stoichiometry (entry 24).

## Perfluoroalkylations of Electron-Rich (Hetero)arenes

With optimized conditions in hand, the trifluoromethylation of a number of electron-rich arenes and heterocycles was performed using 4-phenylpyridine *N*-oxide (**1**; Scheme 2A). The **1**/TFAA adduct exhibited peak reduction at  $-0.91$  V versus SCE in MeCN, which is 190 mV more positive than the measured reduction potential of the pyridine *N*-oxide adduct ( $E_{\text{red}} = -1.10$  V versus SCE in MeCN; see also Figures S34 and S35). Notably, reaction times were significantly shorter when using **1**, and substrate was generally consumed within 2–6 hr. Yields for electron-rich heterocycles were particularly high, and yields of trifluoromethylated products were significantly improved over our previous efforts (up to 28%). Five-membered heterocycles were particularly amenable to the reaction conditions, and acid-labile Boc groups were unaffected by the use of TFAA. In addition, methyliminodiacetic acid (MIDA)-protected boronate esters were well tolerated.<sup>66</sup> The MIDA boronate substrates generally required longer reaction times (12–15 hr) because the conversion of the final 5%–10% of the substrate proceeded slowly. This could be partially overcome through the use of additional equivalents of the *N*-oxide/anhydride reagent. Regardless, remaining starting material for the MIDA boronate substrates invariably co-eluted with the trifluoromethylated products, causing full conversion—and consequently longer reaction times—to be essential for the isolation of clean material. The trifluoromethylated pyrrole **9a** was subjected to an efficient, diastereoselective hydrogenation reaction to provide the trifluoromethylated proline derivative **17** (Scheme 2B), which has been proposed as a potential isostere of pyroglutamic acid.<sup>67</sup>

We next turned our attention to alternative perfluoroalkylation reactions through the use of pentafluoropropionic anhydride (PFPA), which resulted in efficient perfluoroethylation of select substrates in higher yields than the corresponding trifluoromethylations (Scheme 3). Although the reasons behind the differing relative efficiencies of these two processes are not currently understood, the  $\text{CF}_3$  and  $\text{C}_2\text{F}_5$  radicals have been demonstrated to possess surprisingly different kinetic profiles for a number of addition reactions.<sup>68</sup> The reduction potential of the **1**/PFPA adduct was measured to be  $-0.88$  V versus SCE in MeCN, which is not significantly different from the analogous TFAA adduct (see also Figure S36). Most higher-order radical perfluoroalkylation reactions involve the use of perfluoroalkyl iodides,<sup>6</sup> which are generally synthesized from the corresponding fluorinated acids.<sup>69,70</sup>

Expansion of this methodology for the generation of larger perfluoroalkyl radicals predictably becomes less atom-economical as larger and larger acid equivalents are produced as byproducts. Although smaller acid chlorides are volatile ( $\text{F}_3\text{CCOCl}$  bp =  $-27^\circ\text{C}$ ;  $\text{F}_5\text{C}_2\text{COCl}$  bp =  $7^\circ\text{C}$ – $9^\circ\text{C}$ ), the use of heptafluorobutyryl chloride **22** in place of its corresponding anhydride **23** ( $E_{\text{red}}$  of the **1/23** adduct =  $-0.93$  V versus SCE in MeCN; see also Figure S37) provided a comparable yield of pyrrole **24** (Scheme 4). The slightly lower yield obtained with the acid chloride can likely be attributed to incomplete solubility of the reagent in solution.

## Mechanistic Investigations

With particular interest in elucidating the mechanism of the light-promoted trifluoromethylation background reaction (Table 1, entries 21 and 22), we turned our

attention to the absorption of light by other species in solution. At 0.4 M concentration and in the absence of catalyst, the reaction solution containing **1**, TFAA, and mesitylene (**2**) displayed a significant absorbance peak centered at 390 nm, which trailed significantly into the upper 400 nm range (Figure 1A). This absorbance was found to be highly concentration dependent and diminished significantly at lower concentrations (see Supplemental Information). Mesitylene (**2**) and TFAA predictably displayed no absorbance in the visible region of the spectrum, with strictly baseline absorbance above 350 nm. 4-Phenylpyridine *N*-oxide **1** showed an absorbance profile trailing into the visible region, and this absorbance was not significantly altered in the presence of **2**. A mixture of TFAA and **1** in a 1.1:1.0 ratio displayed significant absorbance in the visible region, and a closer analysis provided a number of mechanistically relevant insights.

Because light absorption depends on the presence of TFAA, the relative equivalents of TFAA were varied in the presence of 1.0 equiv of **1** at 0.4 M concentration in MeCN (Figure 1B). The solution displayed the largest absorbance in the visible region when near-equimolar amounts (0.5–1.1 equiv) of TFAA were used and exhibited shifting  $\lambda_{\text{max}}$  values depending on the quantities of TFAA used. Upon the addition of larger amounts (2–8 equiv), the absorbance of the solution stabilized at 367 nm, and subtle changes in absorbance shape were likely due to solvent effects from large excesses of TFAA. These results suggest that the acylation of **1** is a process in equilibrium, which can be forced toward complete acylation through the use of excess TFAA. Although this equilibrium behavior was expected, the large absorbance signals observed in the presence of less TFAA merited closer attention.

To further study this phenomenon, we investigated the possible interaction of the substrate with the fully acylated reagent. The combination of **1**, **2**, and TFAA (1:1:2 ratio; Figure 2A) revealed a strongly absorbing signal in the visible region, and we postulated that this new absorbance could be attributed to an electron donor-acceptor (EDA) interaction.<sup>71</sup> To probe this relationship further, we measured the absorbance profile of the acylated reagent with a number of electron-rich arenes of known ionization potential ( $I_p$ ), including naphthalene ( $I_p = 8.12$  eV),<sup>72</sup> 1,3,5-trimethoxybenzene ( $I_p = 7.96$  eV),<sup>73</sup> and 2-methoxynaphthalene ( $I_p = 7.80$  eV).<sup>74</sup> EDA complexes have a characteristically linear relationship between their charge-transfer absorbance energy ( $h\nu_{\text{CT}} \propto \lambda_{\text{max}}$ ) and the ionization potential ( $I_p$ ) of the constituent donor.<sup>75</sup> The absorbance of the reagent and mesitylene ( $I_p = 8.39$  eV)<sup>76</sup> combination was found to be energetically co-linear with the  $h\nu_{\text{CT}}$  of the other arenes tested (Figure 2B), providing strong evidence for an EDA interaction.

With significant evidence for the presence of EDA interactions in this reagent system, the large, red-shifted absorbance profiles in the absence of substrate (Figure 1B) may be partially explained by analogy. A large excess of TFAA minimizes the broad absorbance of the reagent mixture in the visible region, whereas fewer equivalents result in the highest magnitude of absorbance. We tentatively propose that these absorbance signals represent an EDA interaction between acylated and non-acylated pyridine *N*-oxide, the latter of which is almost fully consumed upon the addition of 2.0 equiv of TFAA. This is, however, an oversimplified mechanistic picture, given that the shifting values of  $\lambda_{\text{max}}$  (and consequently  $h\nu_{\text{CT}}$ ) between 0.5 and 1.1 equiv of TFAA imply a more fundamental structural change than the simple equilibrium of two distinct chemical states. It is possible that oligomeric



complexation is occurring, in which multiple EDA complexes form macromolecular architectures with altered photophysical properties. Further efforts to elucidate this process are currently underway.

EDA complexes have found a number of elegant applications in organic synthesis; for example, a number of leading examples from Melchiorre detail the ability to utilize these interactions in lieu of a photocatalyst.<sup>77–81</sup> For this work, although a significant background reaction was observable for mesitylene (Table 1, entries 20 and 21), the EDA background reaction was not general and was largely dependent on the substrate ionization potential (Figure 2). For example, benzene ( $I_p = 9.24$  eV)<sup>76</sup> displayed no EDA complex absorbance in the visible spectrum, and only the absorbance of the fully acylated reagent could be observed at reaction concentrations. As a consequence, although the use of photocatalyst provided trifluorotoluene in a 73% yield, the reaction without photocatalyst and with 2.0 equiv of TFAA provided merely 11% yield upon irradiation with blue light (Scheme 5). This background reactivity is likely due to direct absorbance of light by the fully acylated reagent, and we further investigated this possibility through irradiation at longer wavelengths where the reagent does not absorb. Interestingly, when green light (510–520 nm) was used instead of blue light, the background reactivity without catalyst dropped significantly and was undetectable for benzene.

EDA complexes undergo photoinduced electron transfer on irradiation on an extremely fast timescale.<sup>82</sup> Although intramolecular donor-acceptor dyads have been used as photosensitizers,<sup>83</sup> literature precedence suggests that the photoexcited state of the intermolecular EDA complexes in question are extremely short lived, to the point where productive intermolecular collisions with the photoexcited state are not likely to occur. Lorance et al.<sup>84</sup> have studied the rates of back-electron transfer and fragmentation for a series of reduced *N*-methoxypyridinium analogs and report impressively fast rates for each of these processes. Specifically, reduced *N*-methoxy-4-phenylpyridinium demonstrated rates of back-electron transfer and fragmentation of  $1.5 \times 10^{12}$  s<sup>-1</sup> and  $2.7 \times 10^{11}$  s<sup>-1</sup>, respectively. Such processes are faster than the limits of diffusion; therefore, the likelihood of productive intermolecular catalysis without a built-in fragmentation pathway with these complexes is small.

Mechanistically, a complex picture emerges from the data. In the presence of TFAA, **1** is acylated, although this event is an equilibrium that is moderately populated on either side of the equation unless an excess of TFAA (1.1 equiv) is used (Scheme 6). This acylated species can readily quench the photoexcited catalyst Ru<sup>2+\*</sup>, and the reduced reagent proceeds to fragment to a carboxyl radical along with 4-phenylpyridine (PhPyr). The carboxyl radical readily extrudes CO<sub>2</sub> to form the CF<sub>3</sub> radical as the key reactive intermediate. In addition to the Ru(bpy)<sub>3</sub>Cl<sub>2</sub>-mediated pathway, the reaction may also proceed through the photoexcitation of EDA complexes in solution, which we propose may arise via complexation of the acylated pyridine-*N*-oxide derivative **25** with either an additional equivalent of **1** or with a sufficiently electron-rich arene such as **2**. Photoexcitation of either complex prompts intermolecular electron transfer, which can either be rendered unproductive through back-electron transfer or proceed toward product by prompting the fragmentation of the acylated reagent to form the CF<sub>3</sub> radical. Subsequent

addition to an electron-rich pi system results in selective formation of the product after re-aromatization. Re-aromatization may occur through oxidation and deprotonation of the substrate or through the reverse sequence.<sup>85</sup>

A final mechanistic consideration is whether propagative behavior is significantly operative in the reaction. Measurement of the quantum yield under irradiation at 436 nm revealed a quantum yield ( $\Phi$ ) of 0.87, signifying that less than 1 equiv of product is produced by every photon absorbed by the reaction.<sup>86</sup> Although this does not conclusively determine that no propagation occurs in the reaction, it is likely that the re-aromatic oxidation to form product is accomplished by the photocatalyst or an oxidized arene such as **1**<sup>+</sup> or **2**<sup>+</sup> rather than by another equivalent of **25**.

### Application on a Kilogram Scale

At the inception of this project, one of the key goals was to demonstrate a scalable methodology to access trifluoromethylated substrates in up to kilogram quantities. Our original report included a reaction run at 18.3 g scale in a flow system, because it was shown that reaction with 100 g in a batch did not surpass 35% conversion (3.3 mmol hr<sup>-1</sup>). Upon further investigation, including determination of the quantum yield to be <1,<sup>87</sup> we surmised that a high photon flux was required to achieve high conversions with reasonable reaction times in flow. Currently available commercial flow systems are capable of providing this increased flux; however, limited reactor volumes limit productivity, and a prohibitive economic penalty is associated with scaling out.<sup>88–90</sup> The original design of a continuous flow reactor for UV photochemistry by Berry, Booker-Milburn, and coworkers.<sup>91</sup> has proven general for visible-light irradiation, and there have been several recent examples.<sup>92–94</sup> This method appears to be the most promising avenue for conducting visible-light reactions at a preparative scale on complex substrates, as shown by a series of pioneering examples by Merck, most notably for the synthesis of elbasvir.<sup>95</sup> Following this general template, we constructed our reactor within the design principles of low cost, easy construction from commercially available parts, and that it should fit within a standard walk-in fume hood.<sup>96</sup> The reactor consisted of blue LED lights contained within a glass beaker wrapped with a single layer of perfluoroalkoxy (PFA) tubing (1.6 mm inner diameter) around the outside, giving a volume of approximately 150 mL (Figure 3A, see also Figures S1 and S2). This assembly was housed within a steel casing with both cavities fully filled with water to provide both cooling of the lights and control of the reaction temperature. Although LED lights are generally considered to have low energy consumption, they can still generate significant heat. In our experience on a larger scale, the use of water provides a more efficient and controllable cooling method than air, which is commonly used on a small scale. Finally, we utilized peristaltic pumps because of their relative low cost and proven reliability over extended operating times.

We chose to demonstrate the viability of this reactor by using Boc-pyrrole substrate **9** and conditions employing pyridine *N*-oxide, because all the reagents could be obtained at the quantities required for a kilogram scale (Figure 3B). Using 0.1 mol % Ru(bpy)<sub>3</sub>Cl<sub>2</sub> and 2.0 equiv of the pyridine *N*-oxide/TFAA adduct, a residence time of 30 min at 45°C was optimal to provide a balance of productivity and conversion, leading to internal assay yields of 60%–



65% with <10% of the starting material remaining. These conditions were operated continuously<sup>97</sup> for 48 hr to process 1.2 kg of pyrrole **9**, and assay yields remained constant between 60% and 65%, representing a consumption of **9** of 25 g hr<sup>-1</sup> (109 mmol hr<sup>-1</sup>; Figure 4). After workup and isolation, 0.95 kg of pyrrole **9a** (81% purity and 50% yield) was obtained, providing a final productivity of 87.2 mmol hr<sup>-1</sup>, which greatly surpassed our previous demonstrations in both batch (4.2 mmol hr<sup>-1</sup>) and flow (14.2 mmol hr<sup>-1</sup>). Furthermore, the useful pyrrole building block **26** could be obtained in >98% purity as a crystalline solid after an unoptimized Boc deprotection in 77% yield (Figure 3C).<sup>98</sup> The demonstration of productivity close to 0.5 kg per day<sup>99</sup> clearly defines this as a proof of concept for the scale-up of visible-light photochemical reactions in flow using simple equipment. The limiting factor of this reactor's construction was the requirement for high photon flux and the necessity that the lights be available commercially. Preliminary studies have indicated that a reactor with increased internal reflectance provides a decreased residence time (30–20 min). Furthermore, a customizable light source of higher photon flux may allow an increased inner diameter (leading to an increased reactor volume), further boosting productivity.<sup>100</sup> Finally, because of the relatively low cost of this reactor, scaling out to meet higher production requirements could be economically viable.

## Conclusion

The utility of pyridine *N*-oxides as safe, practical, and inexpensive reagents for the scalable decarboxylation of TFAA under mild reaction conditions has been demonstrated. The nature of the pyridine moiety has been shown to exert a profound influence on the reaction mechanism, given that further conjugation and electrophilicity of the pyridinium ring system promotes the formation of photoactive EDA complexes. This mechanistic insight has the potential to eliminate the need for transition-metal complexes in this methodology, and further research into this possibility is underway.

## EXPERIMENTAL PROCEDURES

### General Trifluoromethylation Procedure

To a 2 dram vial equipped with a stir bar was added 4-phenylpyridine *N*-oxide (0.8–3.2 mmol, 1.0–4.0 equiv) and substrate (0.80 mmol) followed by 500  $\mu$ L of a 1.2 mg/mL solution of Ru(bpy)<sub>3</sub>Cl<sub>2</sub>·6H<sub>2</sub>O (0.6 mg, 0.1 mol %) in MeCN. The combined materials were then diluted with dry MeCN (1.5 mL, total volume 2 mL MeCN) and stirred briefly to form a heterogeneous solution; the *N*-oxide was only partially dissolved when it was used in higher equivalents. The reaction was sparged with nitrogen gas for 30 s with a glass pipette, and then trifluoroacetic anhydride (0.88–3.28 mmol, 1.1–4.1 equiv) was added under a stream of nitrogen before the vial was quickly sealed with a rubber-lined screw-on cap. The trifluoroacetic anhydride solubilized any remaining solid *N*-oxide within seconds to minutes. Three 4.4 WLED light strips were turned on, and the reactions were allowed to proceed for 3–12 hr before removal of the light source (see Figure S3 for the geometry of the LED setup). Upon completion of the reaction, trifluorotoluene (98  $\mu$ L, 0.80 mmol) was added as a stoichiometric internal standard. A sample of the reaction was removed and diluted with CDCl<sub>3</sub> for nuclear magnetic resonance (NMR) analysis, and the trifluorotoluene signal was referenced to  $\delta = -63.72$ . Workup conditions were substrate dependent.

**9a: 1-(*tert*-Butyl) 2-Methyl 5-(Trifluoromethyl)-1*H*-pyrrole-1,2-dicarboxylate**

After the general procedure, using 4-phenylpyridine *N*-oxide (273.9 mg, 1.6 mmol, 2.0 equiv) and TFAA (237  $\mu$ L, 1.68 mmol, 2.1 equiv), the reaction was run for 3 hr.  $^{19}\text{F}$  NMR analysis of the crude reaction mixture versus the injected trifluorotoluene standard revealed the title compound in a 63% yield. The reaction was partitioned with 1 N HCl and diluted with dichloromethane. The organic phase was separated, washed with saturated  $\text{NaHCO}_3$  and brine, and dried over sodium sulfate before filtering and concentrating. The crude reaction mixture was purified on silica gel with 10%–30% dichloromethane in hexanes to yield the title compound as a clear oil.

Yield: 0.140 g (60%);  $^1\text{H}$  NMR (700 MHz,  $\text{CDCl}_3$ ):  $\delta$  = 6.80 (d,  $J$  = 3.8 Hz, 1H), 6.61 (d,  $J$  = 3.8 Hz, 1H), 3.87 (s, 3H), 1.61 (s, 9H);  $^{19}\text{F}$  NMR (470 MHz,  $\text{CDCl}_3$ ):  $\delta$  = -59.66;  $^{13}\text{C}$  NMR (175 MHz,  $\text{CDCl}_3$ ):  $\delta$  = 160.2, 147.2, 127.8, 125.6 (q, JC-F = 125.6 Hz), 119.9 (q, JC-F = 267 Hz), 116.1, 112.8 (q, JC-F = 3.6 Hz), 86.9, 52.1, 27.1; high-resolution mass spectrometry (EI+)  $m/z$ :  $[\text{M} - \text{Boc} + \text{H}]^+$  calculated 193.0351, found 193.0351. IR (neat):  $\nu$  = 2,989, 1,777, 1,728, 1,558, 1,373, 1,247, 1,123.

**Supplementary Material**

Refer to Web version on PubMed Central for supplementary material.

**Acknowledgments**

We thank Martin Johnson and Jennifer McClary Groh for general discussion about the construction of the flow reactor and calculation of the heat output of the light. We thank John Howell for preparation of pyrrole **9**. We thank Adam McFarland and Jonas Buser for NMR assistance and Dr. Jeff Kampf for X-ray crystallographic analysis. We acknowledge the financial support for this research from the NIH NIGMS (R01-GM096129), the Camille Dreyfus Teacher Scholar Award Program, Eli Lilly and Co., the University of Michigan, and a Lilly Innovation Fellowship Award to J.J.D. from Eli Lilly and Co.

**REFERENCES AND NOTES**

1. Müller K, Faeh C, Diedrich F. Fluorine in pharmaceuticals: looking beyond intuition. *Science*. 2016; 317:1881–1886.
2. Jeschke P. The unique role of fluorine in the design of active ingredients for modern crop protection. *ChemBioChem*. 2004; 5:570–589.
3. Hagman WK. The many roles for fluorine in medicinal chemistry. *J. Med. Chem.* 2008; 51:4359–4368. [PubMed: 18570365]
4. Wang JW, Sánchez-Roselló M, Aceña JL, del Pozo C, Sorochinsky AE, Fustero S, Soloshonok VA, Liu H. Fluorine in pharmaceutical industry: fluorine-containing drugs introduced to the market in the last decade (2001–2011). *Chem. Rev.* 2014; 114:2432–2506. [PubMed: 24299176]
5. Siegemund, G., Schwertfeger, W., Feiring, A., Smart, B., Behr, F., Vogel, H., McKusick, B. Fluorine compounds, organic. In: Elvers, B., editor. *Ullmann's Encyclopedia of Industrial Chemistry*. Wiley; 2000. [http://dx.doi.org/10.1002/14356007.a11\\_349.pub2](http://dx.doi.org/10.1002/14356007.a11_349.pub2)
6. Tomoshenko OA, Grushin VV. Aromatic trifluoromethylation with metal complexes. *Chem. Rev.* 2011; 111:4475–4521. [PubMed: 21456523]
7. Alonso C, de Marigorta EM, Rubiales G, Palacios F. Carbon trifluoromethylation reactions of hydrocarbon derivatives and heteroarenes. *Chem. Rev.* 2015; 115:1847–1935. [PubMed: 25635524]
8. Prakash GKS, Mandal M. Nucleophilic trifluoromethylation tamed. *J. Fluorine Chem.* 2001; 112:123–131.

9. Langlois BR, Billard T, Roussel S. Nucleophilic trifluoromethylation: some recent reagents and their stereoselective aspects. *J. Fluorine Chem.* 2005; 126:173–179.
10. Rubiales G, Alonso C, de Marigorta EM, Palacios F. Nucleophilic trifluoromethylation of carbonyl compounds and derivatives. *ARKIVOC.* 2014; ii:362–405.
11. Liu X, Xu C, Wang M, Liu Q. Trifluoromethyltrimethylsilane: nucleophilic trifluoromethylation and beyond. *Chem. Rev.* 2015; 115:683–730. [PubMed: 24754488]
12. Prakash GKS, Hu J. Selective fluoroalkylations with fluorinated sulfones, sulfoxides, and sulfides. *Acc. Chem. Res.* 2007; 40:921–930. [PubMed: 17708659]
13. Prakash GKS, Krishnamurti R, Olah GA. Synthetic methods and reactions. 141. Fluoride-induced trifluoromethylation of carbonyl compounds with trifluoromethyltrimethylsilane (TMS-CF<sub>3</sub>). A trifluoromethide equivalent. *J. Am. Chem. Soc.* 1989; 111:393–395.
14. Prakash GKS, Wang Y, Mogi R, Hu J, Mathew T, Olah GA. Nucleophilic perfluoroalkylation of imines and carbonyls: perfluoroalkyl sulfones as efficient perfluoroalkyl-transfer motifs. *Org. Lett.* 2010; 12:2932–2935. [PubMed: 20518520]
15. Prakash GKS, Zhang Z, Wang F, Munoz S, Olah GA. Nucleophilic trifluoromethylation of carbonyl compounds: trifluoroacetaldehyde hydrate as a trifluoromethyl source. *J. Org. Chem.* 2013; 78:3300–3305. [PubMed: 23425346]
16. Charpentier J, Früh N, Togni A. Electrophilic trifluoromethylation by use of hypervalent iodine reagents. *Chem. Rev.* 2015; 115:650–682. [PubMed: 25152082]
17. Shibata N, Matsnev A, Cahard D. Shelf-stable electrophilic trifluoromethylating reagents: a brief historical perspective. *Beilstein J. Org. Chem.* 2010; 6:65. [PubMed: 20703379]
18. Umemoto T, Adachi K, Ishihara S. CF<sub>3</sub> oxonium salts, *O*-(Trifluoromethyl) dibenzofuranium salts: in situ synthesis, properties, and application as a real CF<sub>3</sub><sup>+</sup> species reagent. *J. Org. Chem.* 2007; 72:6905–6917. [PubMed: 17676906]
19. Kieltch I, Eisenberger P, Togni A. Mild electrophilic trifluoromethylation of carbon- and sulfur-centered nucleophiles by a hypervalent iodine(III)-CF<sub>3</sub> reagent. *Angew. Chem. Int. Ed. Engl.* 2007; 46:754–757. [PubMed: 17154193]
20. Allen AE, MacMillan DWC. The productive merger of iodonium salts and organocatalysis: a non-photolytic approach to the enantioselective  $\alpha$ -trifluoromethylation of aldehydes. *J. Am. Chem. Soc.* 2010; 132:4986–4987. [PubMed: 20297822]
21. Koike T, Akita M. Trifluoromethylation by visible-light-driven photoredox catalysis. *Top. Catal.* 2014; 57:967–974.
22. Barata-Vallejo S, Postigo A. Metal-mediated radical perfluoroalkylation of organic compounds. *Coord. Chem. Rev.* 2013; 257:3051–3069.
23. Studer A. A “renaissance” in radical trifluoromethylation. *Angew. Chem. Int. Ed. Engl.* 2012; 51:8950–8958. [PubMed: 22890985]
24. McClinton MA, McClinton DA. Trifluoromethylations and related reactions in organic chemistry. *Tetrahedron.* 1992; 48:6555–6666.
25. Zeng T, Xuan J, Chen J, Lu L, Xiao W. Visible light photoredox catalysis in trifluoromethylation reactions. *Imag. Sci. Photochem.* 2014; 32:415–432.
26. Nagib DA, MacMillan DWC. Trifluoromethylation of arenes and heteroarenes by means of photoredox catalysis. *Nature.* 2011; 480:224–228. [PubMed: 22158245]
27. Pham PV, Nagib DA, MacMillan DWC. Photoredox catalysis: a mild, operationally simple approach to the synthesis of  $\alpha$ -trifluoromethyl carbonyl compounds. *Angew. Chem. Int. Ed. Engl.* 2011; 50:6119–6122. [PubMed: 21604347]
28. Nagib DA, Scott ME, MacMillan DWC. Enantioselective  $\alpha$ -trifluoromethylation of aldehydes via photoredox organocatalysis. *J. Am. Chem. Soc.* 2009; 131:10875–10877. [PubMed: 19722670]
29. Ji Y, Brueckl T, Baxter RD, Fujiwara Y, Seiple IB, Su S, Blackmond DG, Baran PS. Innate C–H trifluoromethylation of heterocycles. *Proc. Natl. Acad. Sci. USA.* 2011; 108:14411–14415. [PubMed: 21844378]
30. Fujiwara Y, Dixon JA, O’Hara F, Daa Funder D, Dixon DD, Rodriguez RA, Baxter RD, Herlé B, Sach N, Collins MR, et al. Practical and innate carbon–hydrogen functionalization of heterocycles. *Nature.* 2012; 492:95–99. [PubMed: 23201691]

31. Li Y, Studer A. Transition-metal-free trifluoromethylaminoxylation of alkenes. *Angew. Chem. Int. Ed. Engl.* 2012; 51:8221–8224. [PubMed: 22833448]
32. Zhang B, Mück-Lichtenfeld C, Daniliuc CG, Studer A. 6-Trifluoromethyl-phenanthridines through radical trifluoromethylation of isonitriles. *Angew. Chem. Int. Ed. Engl.* 2013; 52:10792–10795. [PubMed: 24000125]
33. Yasu Y, Koike T, Akita M. Three-component oxytrifluoromethylation of alkenes: highly efficient and regioselective difunctionalization of C=C bonds mediated by photoredox catalysis. *Angew. Chem. Int. Ed. Engl.* 2012; 51:9567–9571. [PubMed: 22936394]
34. Wilger DJ, Gesmundo NJ, Nicewicz DA. Catalytic hydrotrifluoromethylation of styrenes and unactivated aliphatic alkenes via an organic photoredox system. *Chem. Sci.* 2013; 4:3160–3165.
35. Deng Q, Chen J, Wei Q, Zhao Q, Lu L, Xiao W. Visible-light-induced photocatalytic oxytrifluoromethylation of *N*-allylamides for the synthesis of CF<sub>3</sub>-containing oxazolines and benzoxazines. *Chem. Commun.* 2015; 51:3537–3540.
36. Mizuta S, Verhoog S, Engle KM, Khotavivattana T, O'Duill M, Wheelhouse K, Rassias G, Médebielle M, Gouverneur V. Catalytic hydrotrifluoromethylation of unactivated alkenes. *J. Am. Chem. Soc.* 2013; 135:2505–2508. [PubMed: 23373772]
37. Cho EJ, Senecal TD, Kinzel T, Zhang Y, Watson DA, Buchwald SL. The palladium-catalyzed trifluoromethylation of aryl chlorides. *Science.* 2010; 328:1679–1681. [PubMed: 20576888]
38. Morimoto H, Tsubogo T, Litvinas ND, Hartwig JF. A broadly applicable copper reagent for trifluoromethylations and perfluoroalkylations of aryl iodides and bromides. *Angew. Chem. Int. Ed. Engl.* 2011; 50:3793–3798. [PubMed: 21442711]
39. Mazloomi Z, Bansode A, Benavente P, Lishchynskiy A, Urakawa A, Grushin VV. Continuous process for production of CuCF<sub>3</sub> via direct cupration of fluoroform. *Org. Process. Res. Dev.* 2014; 18:1020–1026.
40. Lishchynskiy A, Novikov MA, Martin E, Escudero-Adán EC, Novák P, Grushin VV. Trifluoromethylation of Aryl and heteroaryl halides with fluoroform-derived CuCF<sub>3</sub>: scope, limitations, and mechanistic features. *J. Org. Chem.* 2013; 78:11126–11146. [PubMed: 23964731]
41. Huiban M, Tredwell M, Mizuta S, Wan Z, Zhang X, Collier TL, Gouverneur V, Passchier J. A broadly applicable [18F] trifluoromethylation of aryl and heteroaryl iodides for PET imaging. *Nat. Chem.* 2013; 5:941–944. [PubMed: 24153372]
42. Li X, Zhao J, Zhang L, Hu M, Wang L, Hu J. Copper-mediated trifluoromethylation using phenyl trifluoromethyl sulfoxide. *Org. Lett.* 2015; 17:298–301. [PubMed: 25541645]
43. Morstein J, Hou H, Cheng C, Hartwig JF. Trifluoromethylation of arylsilanes with [(phen)CuCF<sub>3</sub>]. *Angew. Chem. Int. Ed. Engl.* 2016 <http://dx.doi.org/10.1002/anie.201601163>.
44. Zambardi A, Novikov MA, Martin E, Benet-Buchholz J, Grushin VV. Direct cupration of fluoroform. *J. Am. Chem. Soc.* 2011; 133:20901–20913. [PubMed: 22136628]
45. Novák P, Lishchynskiy A, Grushin VV. Fluoroform-derived CuCF<sub>3</sub> for lowcost, simple, efficient, and safe trifluoromethylation of aryl boronic acids in air. *Angew. Chem. Int. Ed. Engl.* 2012; 51:7767–7770. [PubMed: 22715116]
46. Depecker C, Marzouk H, Trevin S, Devynck J. Trifluoromethylation of aromatic compounds via Kolbe electrolysis in pure organic solvent. Study on laboratory and pilot scale. *New J. Chem.* 1999; 23:739–742.
47. Matsui K, Tobita E, Ando M, Kondo K. A convenient trifluoromethylation of aromatic halides with sodium trifluoroacetate. *Chem. Lett.* 1981; 10:1719–1720.
48. Chen M, Buchwald SL. Rapid and efficient trifluoromethylation of aromatic and heteroaromatic compounds using potassium trifluoroacetate enabled by a flow system. *Angew. Chem. Int. Ed. Engl.* 2013; 52:11628–11631. [PubMed: 24038907]
49. Tanabe Y, Matsuo N, Ohno N. Direct perfluoroalkylation including trifluoromethylation of aromatics with perfluoro carboxylic acids mediated by xenon difluoride. *J. Org. Chem.* 1988; 53:4582–4585.
50. Shi G, Shao C, Pan S, Yu J, Zhang Y. Silver-catalyzed C–H trifluoromethylation of arenes using trifluoroacetic acid as the trifluoromethylating reagent. *Org. Lett.* 2015; 17:38–41. [PubMed: 25517200]

51. Lai C, Mallouk TE. A new approach to the photochemical trifluoromethylation of aromatic compounds. *J. Chem. Soc. Chem. Commun.* 1993:1359–1361.
52. Sawada H, Nakayama M. Trifluoromethylation of aromatic compounds with bis(trifluoroacetyl) peroxide. *J. Fluorine Chem.* 1990; 46:423–431.
53. For a more recent example of this chemistry, see Zhong S, Hafner A, Hussal C, Nieger M, Bräse S. Metal-free radical perfluoroalkylation of (Hetero)arenes. *RSC Adv.* 2015; 5:6255–6258.
54. Zuo Z, Cong H, Li W, Choi J, Fu GC, MacMillan DWC. Enantioselective decarboxylative arylation of  $\alpha$ -amino acids via the merger of photoredox and nickel catalysis. *J. Am. Chem. Soc.* 2016; 138:1832–1835. [PubMed: 26849354]
55. Nawrat CC, Jamison CR, Slutskyy Y, MacMillan DWC, Overman LE. Oxalates as activating groups for alcohols in visible light photoredox catalysis: formation of quaternary centers by redox-neutral fragment coupling. *J. Am. Chem. Soc.* 2015; 137:11270–11273. [PubMed: 26322524]
56. Chu L, Lipshultz JM, MacMillan DWC. Merging photoredox and nickel catalysis: the direct synthesis of ketones by the decarboxylative arylation of  $\alpha$ -oxo acids. *Angew. Chem. Int. Ed. Engl.* 2015; 54:7929–7933. [PubMed: 26014029]
57. Ventre S, Petronijevic FP, MacMillan DWC. Decarboxylative fluorination of aliphatic carboxylic acids via photoredox catalysis. *J. Am. Chem. Soc.* 2015; 137:5654–5657. [PubMed: 25881929]
58. Noble A, McCarver SJ, MacMillan DWC. Merging photoredox and nickel catalysis: decarboxylative cross-coupling of carboxylic acids with vinyl halides. *J. Am. Chem. Soc.* 2015; 137:624–627. [PubMed: 25521443]
59. Zuo Z, MacMillan DWC. Decarboxylative arylation of  $\alpha$ -amino acids via photoredox catalysis: a one-step conversion of biomass to drug pharmacophore. *J. Am. Chem. Soc.* 2014; 136:5257–5260. [PubMed: 24712922]
60. Zuo Z, Ahneman DT, Chu L, Terrett JA, Doyle AG, MacMillan DWC. Merging photoredox with nickel catalysis: coupling of  $\alpha$ -carboxyl sp<sup>3</sup>-carbons with aryl halides. *Science.* 2014; 345:437–440. [PubMed: 24903563]
61. Cassani C, Bergonzini G, Wallentin C-J. Photocatalytic decarboxylative reduction of carboxylic acids and its application in asymmetric synthesis. *Org. Lett.* 2014; 16:4228–4231. [PubMed: 25068198]
62. Griffin JD, Zeller MA, Nicewicz DA. Hydrodecarboxylation of carboxylic and malonic acid derivatives via organic photoredox catalysis: substrate scope and mechanistic insight. *J. Am. Chem. Soc.* 2015; 137:11340–11348. [PubMed: 26291730]
63. Huang H, Jia K, Chen Y. Hypervalent iodine reagents enable chemoselective deboronative/ decarboxylative alkenylation by photoredox catalysis. *Angew. Chem. Int. Ed. Engl.* 2015; 54:1881–1884. [PubMed: 25504966]
64. Beatty JW, Douglas JJ, Cole KP, Stephenson CRJ. A scalable and operationally simple trifluoromethylation. *Nat. Commun.* 2015; 6:7919. [PubMed: 26258541]
65. Boekelheide V, Linn WJ. Rearrangements of *N*-oxides. A novel synthesis of pyridyl carbinols and aldehydes. *J. Am. Chem. Soc.* 1954; 76:1286–1291.
66. Attempts to trifluoromethylate aryltrifluoroborate salts were unsuccessful because of the reactivity of TFAA with fluoride anions. Off-gassing was observed, which is attributed to the formation of CF<sub>3</sub>COF (bp= -59°C). This phenomenon has been previously proposed: Roscales S, Csáky AG. Metal-free ring-opening of epoxides with potassium trifluoroborates. *Chem. Commun.* 2014; 50:454.
67. Kondratov IS, Dolovanyuk VG, Tolmachova NA, Gerus II, Bergander K, Frölich R, Haufe G. Reactions of  $\beta$ -alkoxyvinyl polyfluoroalkyl ketones with ethyl isocyanoacetate and its use for the synthesis of new polyfluoroalkyl pyrroles and pyrrolidines. *Org. Biomol. Chem.* 2012; 10:8778–8785. [PubMed: 22948733]
68. Dolbier WR. Structure, reactivity, and chemistry of fluoroalkyl radicals. *Chem. Rev.* 1996; 96:1557–1584. [PubMed: 11848804]
69. Tarrant P. Fluorocarbon iodides—versatile reagents. *J. Fluorine Chem.* 1984; 25:69–74.
70. Haszeldine RN. The reactions of metallic salts of acids with halogens. Part I. The reaction of metal trifluoroacetates with iodine, bromine, and chlorine. *J. Chem. Soc.* 1951:584–587.



71. Lima CGS, Lima TDM, Duarte M, Jurberg ID, Paixão MW. Organic synthesis enabled by light-irradiation of EDA complexes: theoretical background and synthetic applications. *ACS Catal.* 2016; 6:1389–1407.
72. Yoon KB, Kochi JK. Stepwise assembly of charge-transfer complexes within zeolite supercages as visual probes for shape selectivity. *J. Phys. Chem.* 1991; 95:3780–3790.
73. Verhoeven JW, Dirkx IP, de Boer TJ. Studies of inter- and intra-molecular donor-acceptor interactions—II: intermolecular charge transfer involving substituted pyridinium ions. *Tetrahedron.* 1969; 25:3395–3405.
74. Nagy OB, Dupire S, Nagy JB. New ionization potentials from charge-transfer spectra. *Tetrahedron.* 1975; 31:2453–2456.
75. Lee KW, Kochi JK. Charge-transfer structures of aromatic EDA complexes with *n*-heteroatom-substituted pyridinium cations. *J. Chem. Soc. Perkin Trans.* 1992; 2:1011–1017.
76. Miller LL, Nordblom GD, Mayeda EA. Simple, comprehensive correlation of organic oxidation and ionization potentials. *J. Org. Chem.* 1972; 37:916–918.
77. Arceo E, Jurberg ID, Álvarez-Fernández A, Melchiorre P. Photochemical activity of a key donor-acceptor complex can drive stereoselective catalytic  $\alpha$ -alkylation of aldehydes. *Nat. Chem.* 2013; 5:750–756. [PubMed: 23965676]
78. Wo niak Ł, Murphy JJ, Melchiorre P. Photo-organocatalytic enantioselective perfluoroalkylation of  $\beta$ -ketoesters. *J. Am. Chem. Soc.* 2015; 137:5678–5681. [PubMed: 25901659]
79. Kanukuri SR, Bahamonde A, Chatterjee I, Jurberg ID, Escudero-Adán EC, Melchiorre P. X-ray characterization of an electron donor-acceptor complex that drives the photochemical alkylation of indoles. *Angew. Chem. Int. Ed. Engl.* 2015; 54:1485–1489. [PubMed: 25475488]
80. Arceo E, Bahamonde A, Bergonzini G, Melchiorre P. Enantioselective direct  $\alpha$ -alkylation of cyclic ketones by means of photo-organocatalysis. *Chem. Sci.* 2014; 5:2438–2442.
81. Nappi M, Bergonzini G, Melchiorre P. Metal-free photochemical aromatic perfluoroalkylation of  $\alpha$ -cyano arylacetates. *Angew. Chem. Int. Ed. Engl.* 2014; 53:4921–4925. [PubMed: 24668827]
82. Hilinski EF, Masnovi JM, Amatore C, Kochi JK, Rentzepis PM. Charge-transfer excitation of electron donor-acceptor complexes. Direct observation of ion pairs by time-resolved picosecond spectroscopy. *J. Am. Chem. Soc.* 1983; 105:6167–6168.
83. Luo J, Zhang J. Donor-acceptor fluorophores for visible-light-promoted organic synthesis: photoredox/Ni dual catalytic C(sp<sup>3</sup>)-C(sp<sup>2</sup>) cross-coupling. *ACS Catal.* 2016; 6:873–877.
84. Lorange ED, Kramer WH, Gould IR. Barrierless electron transfer bond fragmentation reactions. *J. Am. Chem. Soc.* 2004; 126:14071–14078. [PubMed: 15506771]
85. Dewanji A, Murarka S, Curran DP, Studer A. Phenyl hydrazine as initiator for direct arene C–H arylation via base promoted homolytic aromatic substitution. *Org. Lett.* 2013; 15:6102–6105. [PubMed: 24251964]
86. Cismesia MA, Yoon TP. Characterizing chain processes in visible light photoredox catalysis. *Chem. Sci.* 2015; 6:5426–5434. [PubMed: 26668708]
87. As previously noted, the reaction also becomes dark, thus further limiting light penetration.
88. The concept of scaling out photochemical reactions has been effectively demonstrated Su Y, Kuijpers K, Hessel V, Noël T. A convenient numbering-up strategy for the scale-up of gas-liquid photoredox catalysis in flow. *React. Chem. Eng.* 2016; 1:73–81.
89. Reis NM, Puma GL. A novel microfluidic approach for extremely fast and efficient photochemical transformations in fluoropolymer microcapillary films. *Chem. Commun.* 2015; 51:8414–8417.
90. Elvira KS, Wootton RCR, Reis NM, Mackley MR, deMello AJ. Through-wall mass transport as a modality for safe generation of singlet oxygen in continuous flows. *ACS Sustain. Chem. Eng.* 2013; 1:209–213.
91. Hook BDA, Dohle W, Hirst PR, Pickworth M, Berry M, Booker-Milburn KI. A practical flow reactor for continuous organic photochemistry. *J. Org. Chem.* 2005; 70:7558–7564. [PubMed: 16149784]
92. Su Y, Straathof NJW, Hessel V, Noël T. Photochemical transformations accelerated in continuous-flow reactors: basic concepts and applications. *Chem. Eur. J.* 2014; 20:10562–10589. [PubMed: 25056280]



93. Cambié D, Bottecchia C, Straathof NJW, Hessel V, Noël T. Applications of continuous-flow photochemistry in organic synthesis, material science, and water treatment. *Chem. Rev.* 2016 <http://dx.doi.org/10.1021/acs.chemrev.5b00707>.
94. Garlets ZJ, Nguyen JD, Stephenson CRJ. The development of visible-light photoredox catalysis in flow. *Isr. J. Chem.* 2014; 54:351–360. [PubMed: 25484447]
95. Yayla HG, Peng F, Mangion IK, McLaughlin MM, Campeau L-C, Davies IW, DiRocco DA, Knowles RR. Discovery and mechanistic study of a photocatalytic indoline dehydrogenation for the synthesis of elbasvir. *Chem. Sci.* 2016; 7:2066–2073.
96. See the Supplemental Information for full details of the reactor design.
97. Pumps were temporarily stopped for <1 min while the feed bottles were refilled.
98. We appreciate that direct trifluoromethylations to form pyrrole **25** have been reported; however, it remains unclear whether those processes could be operated at a kilogram scale. See Baar M, Blechert S. Graphitic carbon nitride polymer as a recyclable photoredox catalyst for fluoroalkylation of arenes. *Chem. Eur. J.* 2015; 21:526–530. [PubMed: 25413695]
99. We use 24 hr to define a day, but it should be appreciated that in many cases, other restrictions may prevent full 24 hr operation on a large (e.g., plant) manufacturing scale.
100. Many visible-light-mediated reactions have higher quantum yields, i.e.,  $\gg 1$  where photon flux may not be the limiting factor. See Luo and Zhang.<sup>83</sup>

**HIGHLIGHTS**

A range of electron-rich heterocycles are perfluoroalkylated in good yields

Mechanistic insights include the formation of electron donor-acceptor complexes

This inexpensive process has been validated on a kilogram scale in a flow reactor

Author Manuscript

Author Manuscript

Author Manuscript

Author Manuscript

### The Bigger Picture

Perfluoroalkyl-containing compounds constitute an essential component for advancements in modern health care and the physical and life sciences, as demonstrated by an impressive cohort of fluorinated pharmaceuticals currently on the market. Current state-of-the-art methods for their manufacture require the use of complex, expensive, or environmentally damaging reagents such as fluoroform (a potent greenhouse gas). To facilitate the large-scale production of high-value fluorochemicals, the development of technologies that utilize inexpensive and environmentally benign fluorocarbon sources is essential. Furthermore, expanding the toolbox of methods for the synthesis of fluorine-containing molecules will facilitate their continued diversity, providing new functionality from this prominent class of compounds. This article details the use of perfluoroacid anhydrides in concert with sustainable visible light, thereby demonstrating a truly scalable alternative to current methods.

Author Manuscript

Author Manuscript

Author Manuscript

Author Manuscript

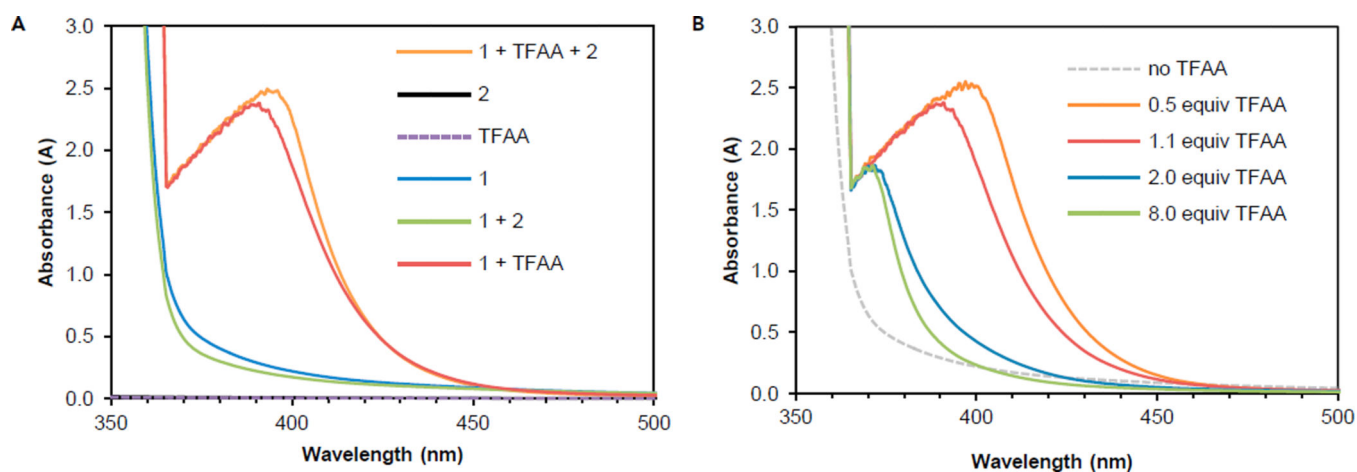


### Figure 1. Optical Absorption Spectra of Individual Reaction Components

Measurements were obtained at experimentally relevant concentrations (0.4 M) in MeCN in 1 cm path quartz cuvettes. See also Figure S33.

(A) Varied combinations of reaction components in the absence of  $\text{Ru}(\text{bpy})_3\text{Cl}_2$ .

Combinations of 4-phenylpyridine *N*-oxide (**1**) and TFAA display strong absorbance in the visible region both in the presence and absence of mesitylene (**2**).

(B) Dramatic changes in absorbance are observed with varied amounts of TFAA in the presence of 1 equiv of **1**.

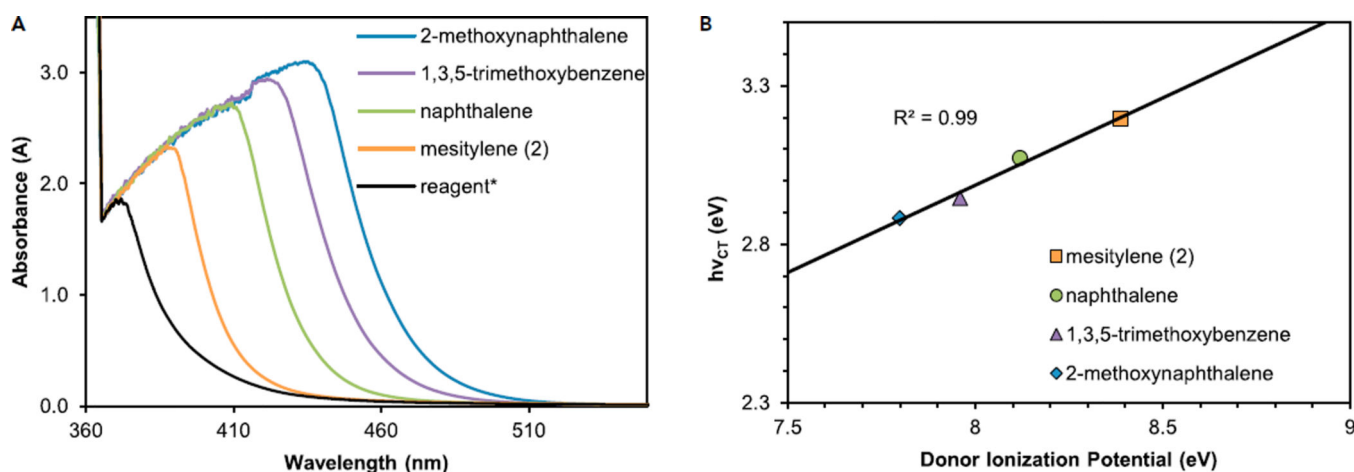


### Figure 2. Evidence for the Formation of EDA Complexes

Measurements were obtained at experimentally relevant concentrations (0.4 M) in MeCN in 1 cm path quartz cuvettes.

(A) Optical absorbance spectra of various electron-rich arenes in the presence of 4-phenylpyridine *N*-oxide (1.0 equiv) and TFAA (2 equiv). \*Reagent indicates the *N*-oxide/TFAA mixture in the absence of an electron-rich arene in solution.

(B) The charge-transfer energy ( $h\nu_{CT}$ ) of each absorbance trends linearly with each donor arene's ionization potential.

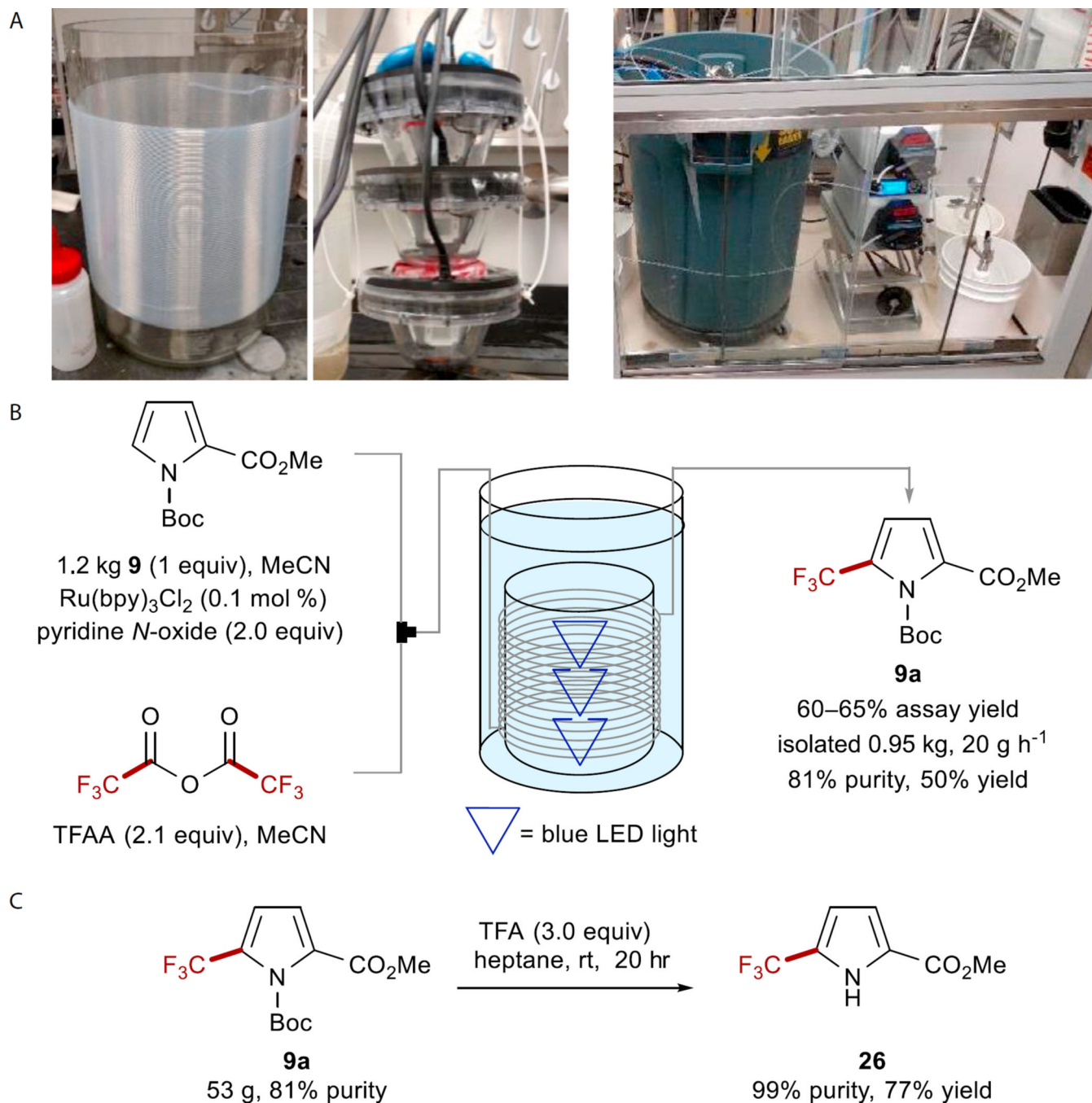


### Figure 3. Kilogram-Scale Trifluoromethylation in Flow

Pyrrrole **9** was subjected to optimized trifluoromethylation conditions on a kilogram scale.

(A) Using a customized flow reactor, 1.2 kg of pyrrole **9** was processed within 48 hr to provide the desired product in a 60%–65% assay yield. The reactor was immersed in water and cooled with a glycol chiller to maintain a steady temperature profile at room temperature. See also Figures S25–S29.

(B) The reactor was constructed from PFA tubing with an internal volume of 150 mL (left). The three blue LEDs (middle) were placed in the middle of the reactor, and the setup was



submerged in the cooling bath and covered during the run (right). See also Figures S1 and S2.

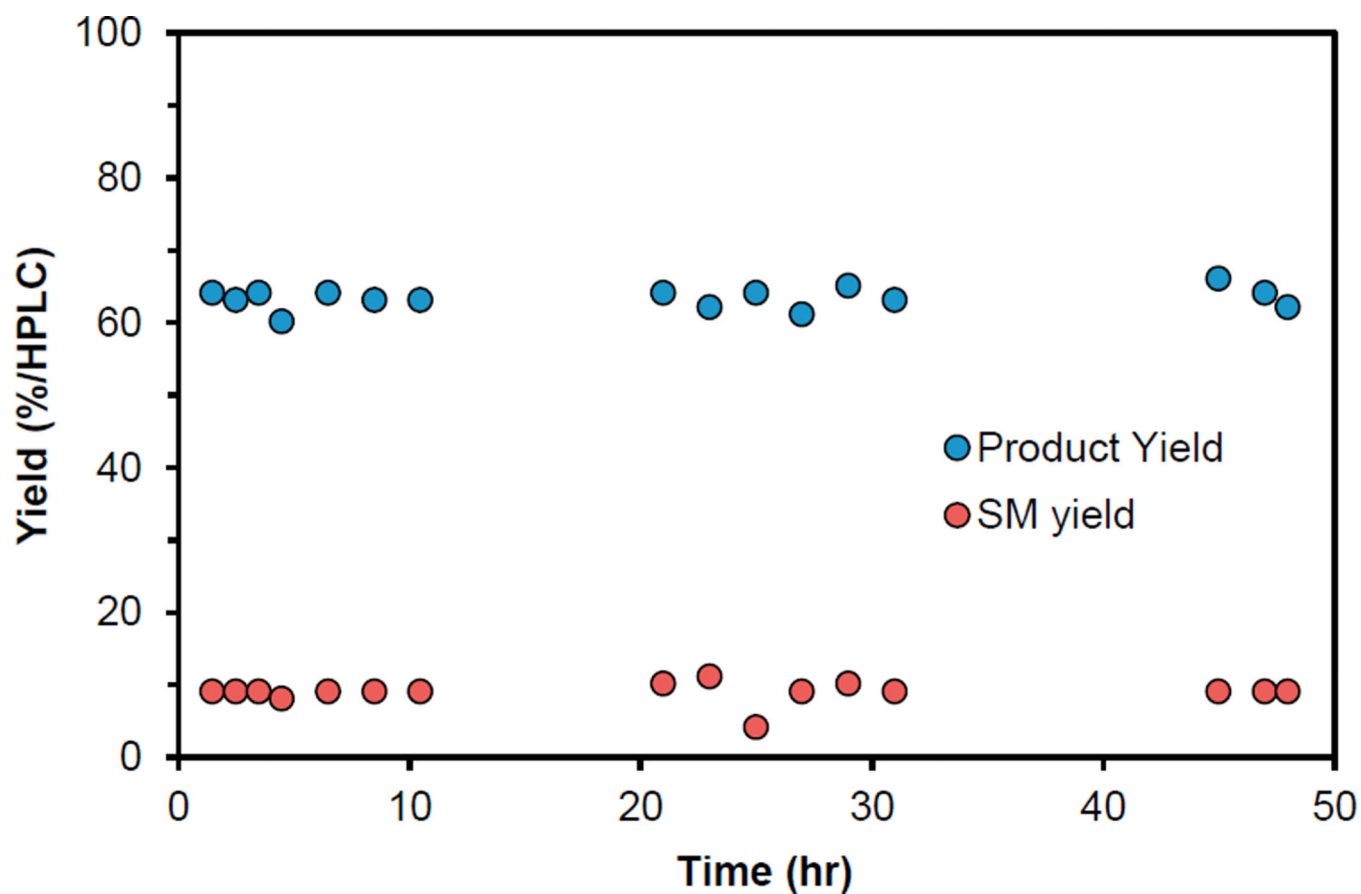
(C) The crude reaction product could be recrystallized to 99% purity after an unoptimized Boc deprotection. See also Figures S31 and S32.

Author Manuscript

Author Manuscript

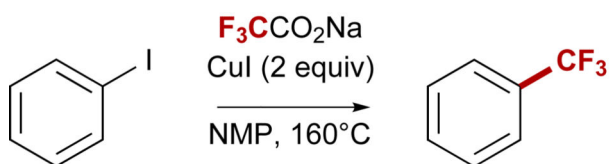
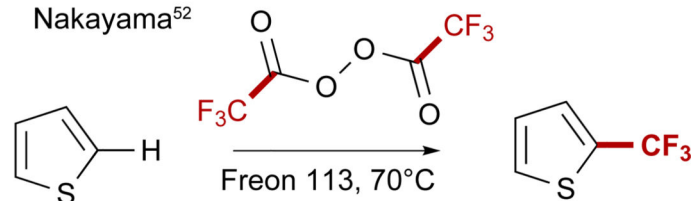
Author Manuscript

Author Manuscript

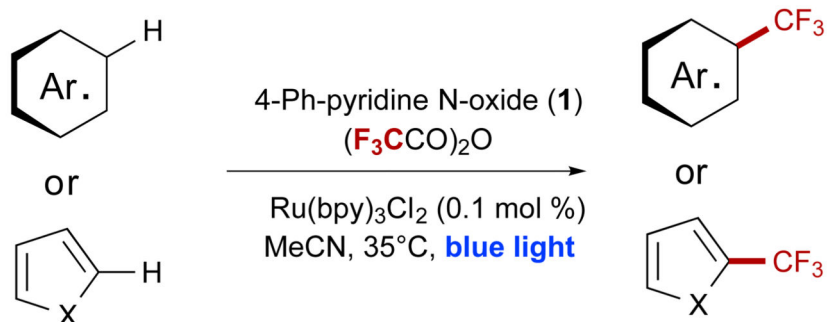
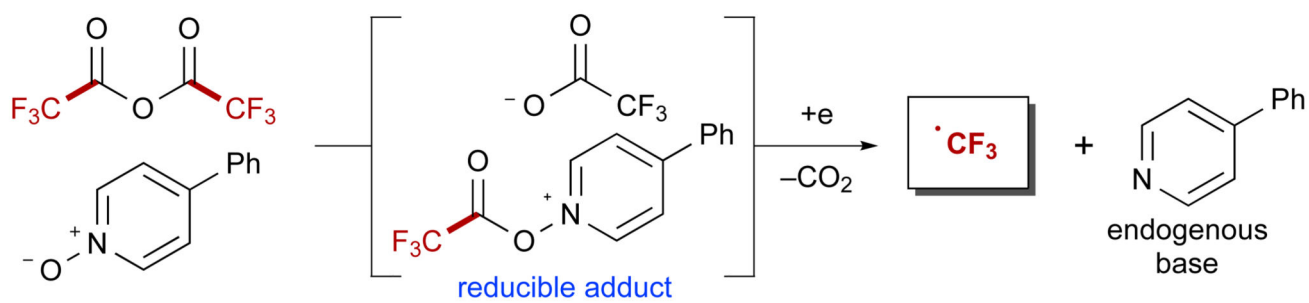


**Figure 4. Reaction Profile over Time**

The reaction was monitored by high-performance liquid chromatography assay over the 48 hr of continuous processing.

Matsui et al.<sup>47</sup>Sawada and Nakayama<sup>52</sup>

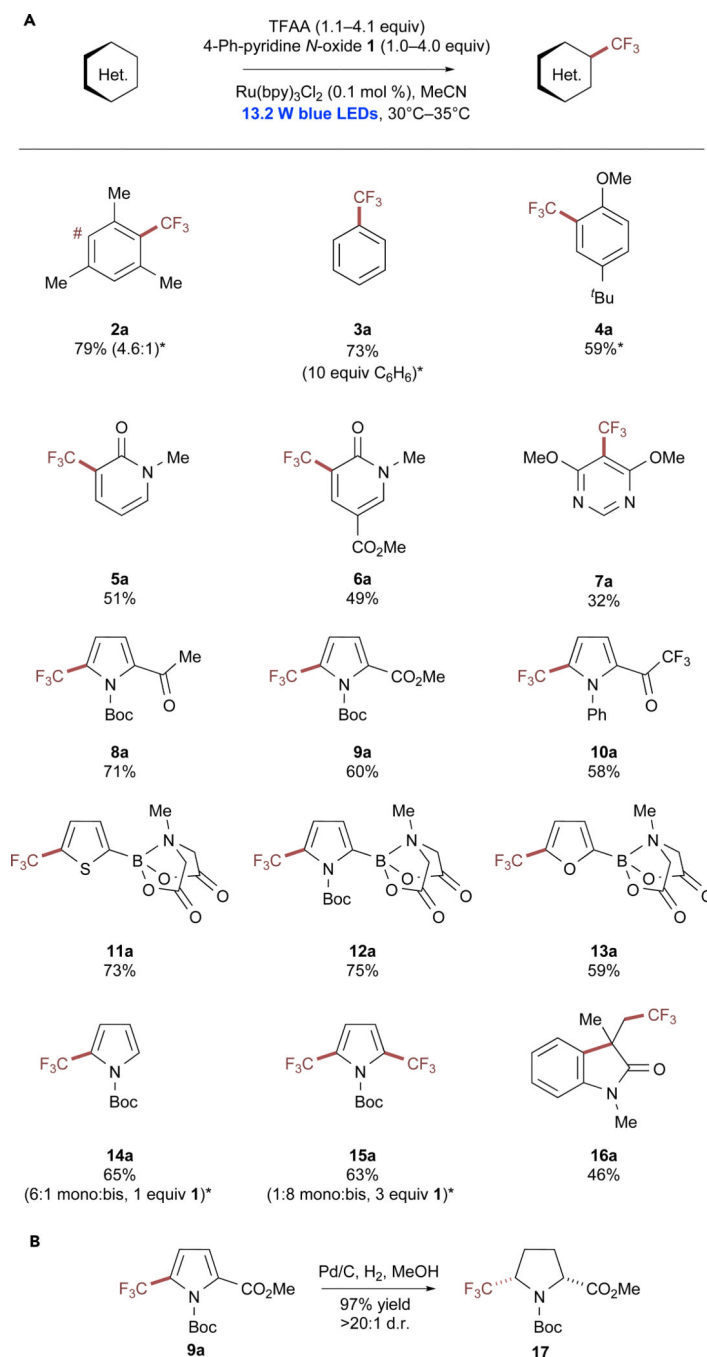
This work:



- inexpensive reagents
- mild reaction conditions
- operationally simple
- demonstrated on Kg scale

**Scheme 1. Strategies for the Decarboxylation of Trifluoroacetate Derivatives**

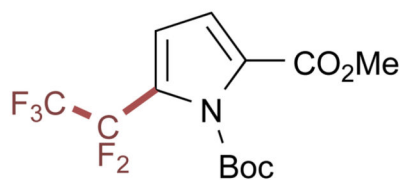
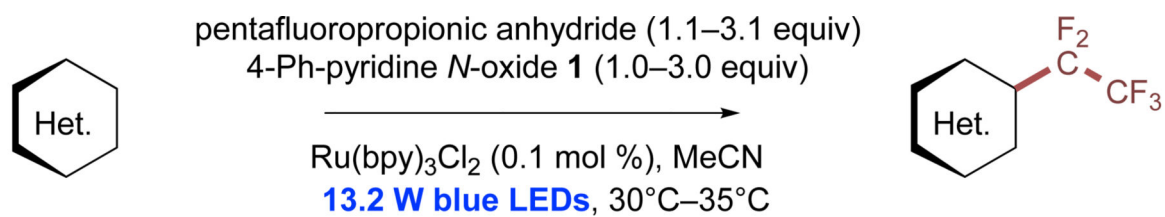
A notable precedent for the decarboxylation of trifluoroacetate derivatives includes the use of superstoichiometric copper and bis(trifluoroacetyl)peroxide. Freon 113 = 1,1,2-trichloro-1,2,2-trifluoroethane.



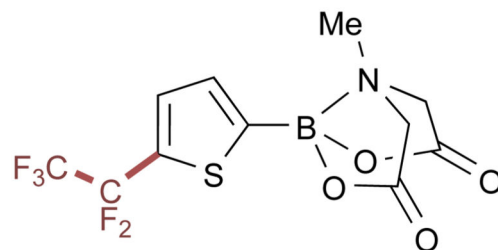
**Scheme 2. Trifluoromethylation of (Hetero)arenes with Trifluoroacetic Anhydride**

(A) Trifluoromethylation of electron-rich substrates with trifluoroacetic acid. All reactions were performed on a 0.8 mmol scale at 0.4 M concentration. Isolated yields are reported in all cases except for instances of product volatility, in which case yields are reported as <sup>19</sup>F NMR internal standard yield. \*Internal standard yield. See also Figures S4–S13.

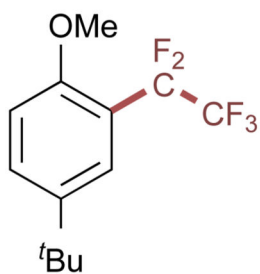
(B) Hydrogenation of pyrrole products can yield high-value perfluoroalkylated pyrrolidines in a diastereoselective fashion. See also Figures S22–S24.



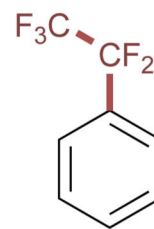
**18**  
72%



**19**  
91%

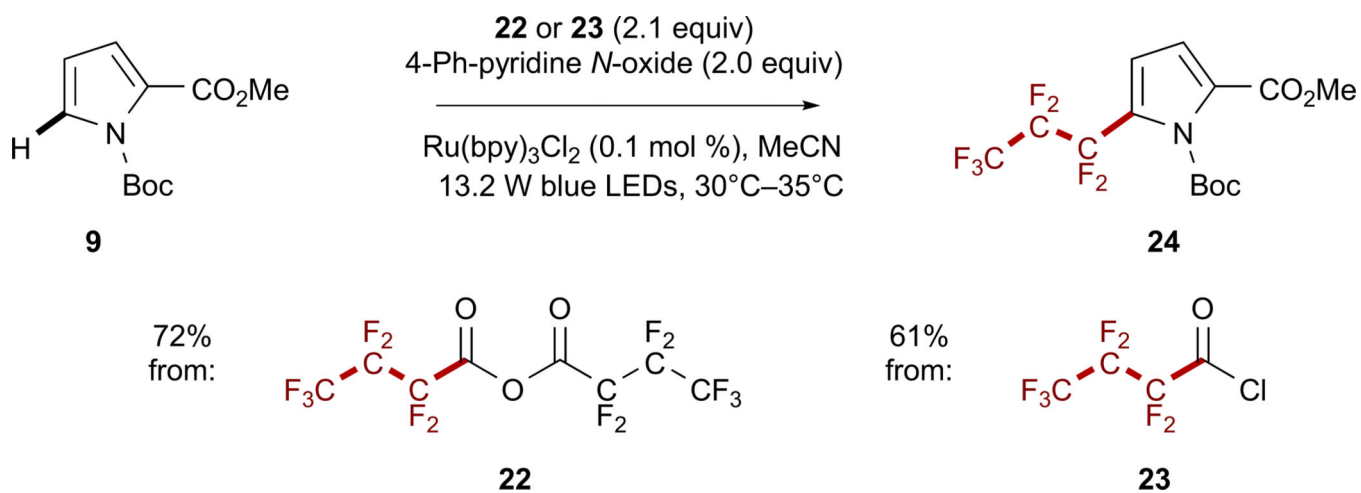


**20**  
81%



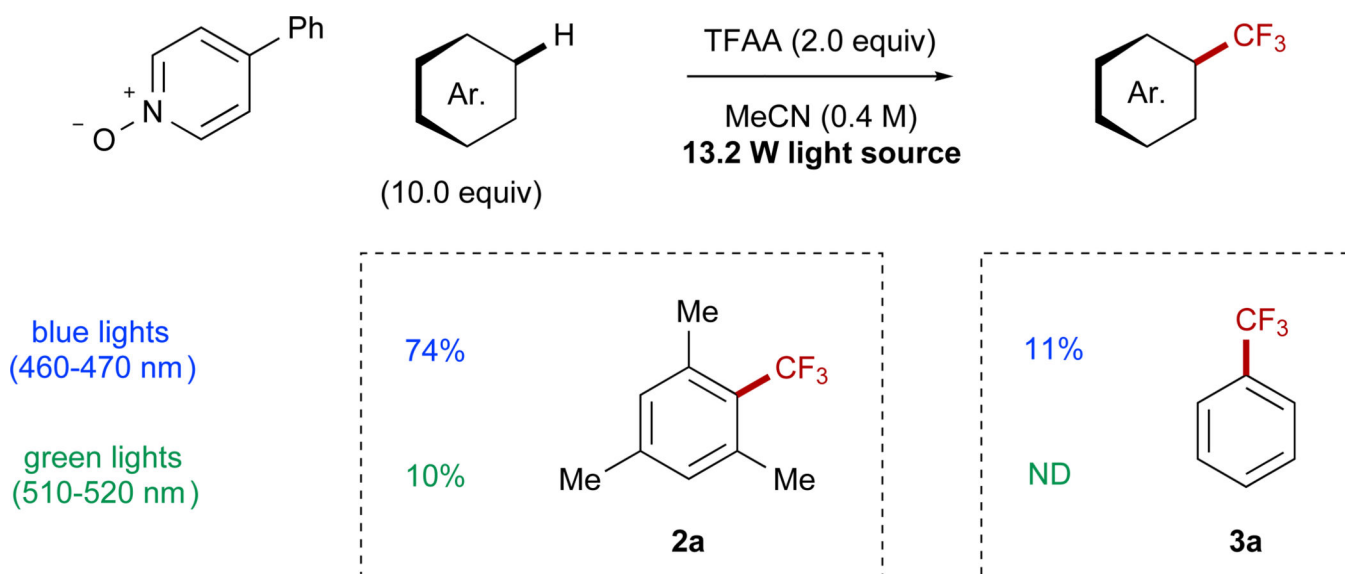
**21**  
83%  
(10 equiv C<sub>6</sub>H<sub>6</sub>)

**Scheme 3. Pentafluoroethylation of (Hetero)arenes with Pentafluoropropionic Anhydride**  
All reactions were performed on a 0.8 mmol scale at 0.4 M concentration. Isolated yields are reported in all cases. See also Figures S14–S19.

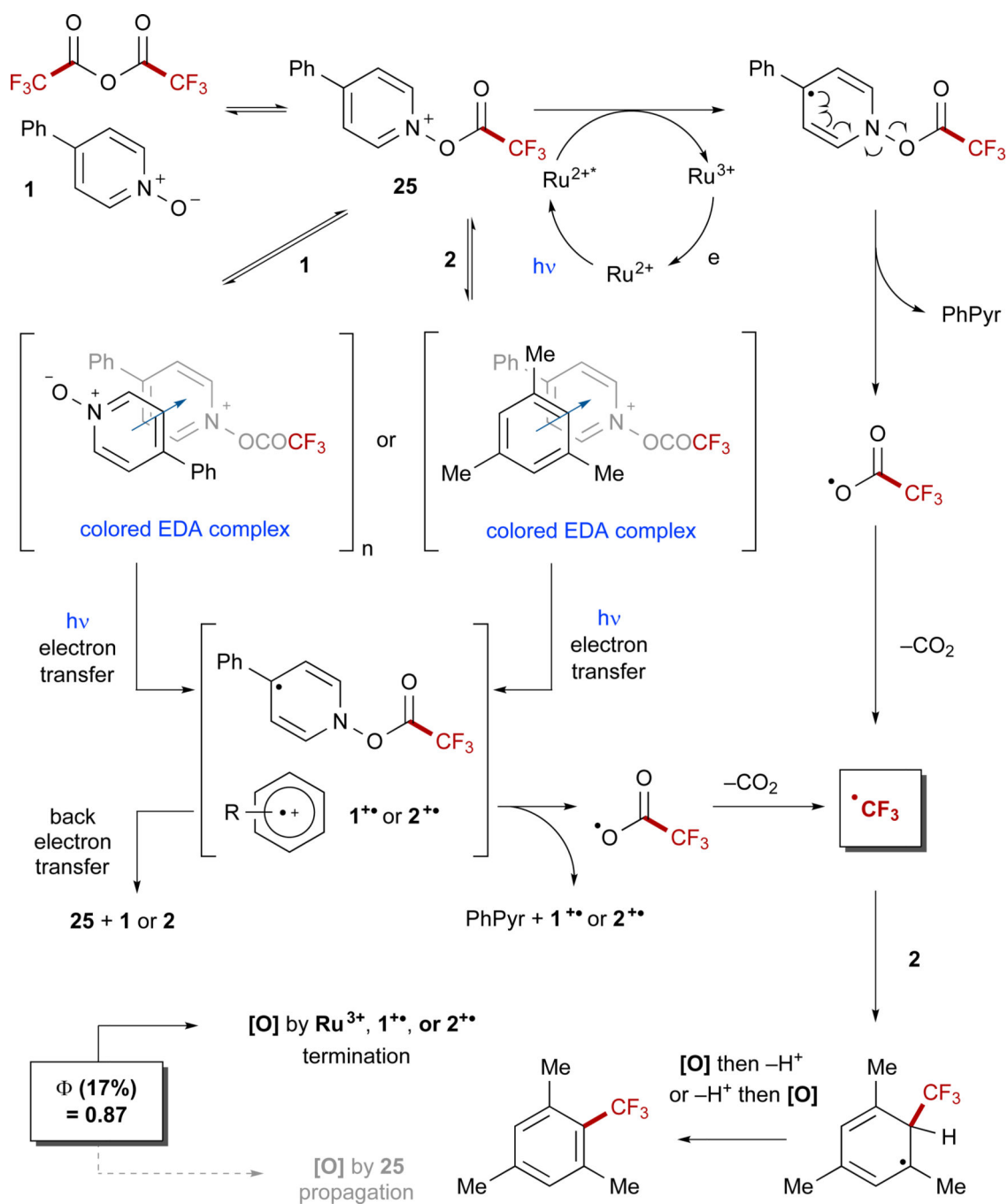
**Scheme 4. Heptafluoropropylation of (Hetero)arenes with Acid Anhydrides and Chlorides**

All reactions were performed on a 0.8 mmol scale at 0.4 M concentration. Isolated yields are reported in all cases. See also Figures S20 and S21.



**Scheme 5. Effects of Wavelength on Reaction Progress**

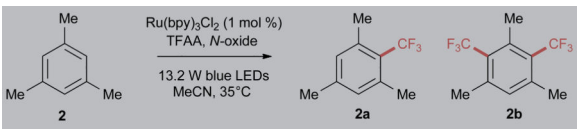
The observed EDA-promoted background reaction is highly substrate specific. See also Figure S25.



### Scheme 6. Mechanistic Proposal

With the formation of EDA complexes in solution, two distinct mechanistic opportunities present themselves for photochemical reaction progress. PhPyr = 4-phenylpyridine. See also Figures S38–S41.

Table 1

Optimization of *N*-Oxide Electronics


Entry <sup>a</sup>	<i>N</i> -Oxide	Equiv <sup>b</sup>	Yield 2a <sup>c</sup>	Yield 2b <sup>c</sup>
1	pyridine	1	44%	<5%
2	4-Cl-pyridine	1	16%	ND
3	4-CN-pyridine	1	25%	<5%
4	4-NO <sub>2</sub> -pyridine	1	ND	ND
5	4- <i>t</i> -Bu-pyridine	1	27%	ND
6	3,5-dimethoxypyridine	1	<10%	ND
7	4-methoxypyridine	1	<10%	ND
8	quinoline	1	ND	ND
9	4-phenylpyridine ( <b>1</b> )	1	54%	<5%
10	2-phenylpyridine	1	24%	<5%
11	2,2'-bipyridine monooxide	1	45%	<5%
12	2,2'-bipyridine bisoxide	0.5 <sup>d</sup>	29%	<5%
13 <sup>e</sup>	pyridine	1	ND	ND
14 <sup>e</sup>	<b>1</b>	1	<10%	ND
15	pyridine	2	47%	<5%
16	<b>1</b>	2	59%	16%
17 <sup>f</sup>	pyridine	2	57%	12%
18 <sup>f</sup>	<b>1</b>	2	62%	16%
19 <sup>f,g</sup>	pyridine	2	57%	6%
20 <sup>f,g</sup>	<b>1</b>	2	65%	14%
21 <sup>e,f</sup>	<b>1</b>	1	40%	<5%
22 <sup>e,f</sup>	<b>1</b>	2	55%	<5%
23 <sup>e,f,h</sup>	<b>1</b>	1	ND	ND
24 <sup>e,f,i</sup>	<b>1</b>	1	74%	<5%

ND, not detected.

<sup>a</sup>Optimization reactions were performed on a 0.8 mmol scale in 2.0 mL of MeCN for a 12 hr reaction time.

<sup>b</sup>For every X equiv of *N*-oxide, X.1 equiv of TFAA was used.

<sup>c</sup>Yields obtained versus trifluorotoluene as <sup>19</sup>F NMR internal standard.

<sup>d</sup>1.1 equiv of TFAA.

<sup>e</sup>No catalyst.

<sup>f</sup>Degassed.

<sup>g</sup>0.1 mol % Ru(bpy)<sub>3</sub>Cl<sub>2</sub>.

<sup>h</sup>Light excluded.

<sup>i</sup>10.0 equiv of mesitylene (**2**).

Author Manuscript

Author Manuscript

Author Manuscript

Author Manuscript